Spin filtering and entanglement detection due to spin-orbit interaction in carbon nanotube cross-junctions

Francesco Mazza,[1,2] Bernd Braunecker,[1] Patrik Recher,[3] and Alfredo Levy Yeyati[1]

[1]*Departamento de Física Teórica de la Materia Condensada, Condensed Matter Physics Center (IFIMAC), and Instituto Nicolás Cabrera, Universidad Autónoma de Madrid, E-28049 Madrid, Spain*
[2]*NEST, Scuola Normale Superiore, and Istituto Nanoscienze-CNR, I-56126 Pisa, Italy*
[3]*Institute for Mathematical Physics, Technical University Braunschweig, Mendelssohnstr. 3, D-38106 Braunschweig, Germany*

We demonstrate that, due to their spin-orbit interaction, carbon nanotube cross-junctions have attractive spin projective properties for transport. First, we show that the junction can be used as a versatile spin filter as a function of a backgate and a static external magnetic field. Switching between opposite spin filter directions can be achieved by small changes of the backgate potential, and a full polarization is generically obtained in an energy range close to the Dirac points. Second, we discuss how the spin filtering properties affect the noise correlators of entangled electron pairs, which allows us to obtain signatures of the type of entanglement that are different from the signatures in conventional semiconductor cross-junctions.

I. INTRODUCTION

Over the last two decades, carbon nanotubes (CNTs) have developed into a mature material that can be produced at high purity,[1–7] and important steps toward mass production have been taken.[8,9] This makes CNTs an attractive platform for a future implementation of quantum information processing or spintronics. In this context, CNTs have already been proven functional for producing correlated electron pairs in a double quantum dot Cooper pair splitter setup.[10,11] Such Cooper pair splitters[12] are first implementations of a source of entangled electron pairs on demand, complementing similar implementations in semiconductors,[13–15] and they are related closely to proposals for generating entangled pairs in systems with forked geometry.[16–25]

To actively control the electron spin, spin-orbit interaction (SOI) effects have found much attention in recent years, since they allow an all-electric local control of the electron spin. While in semiconductors the SOI typically causes the spin to precess during transport, in CNTs, which are hollow cylinders different from filled quantum wires, the SOI has a different impact. Rather than causing spin rotations, it lifts the energy degeneracy of opposite spins and leads to distinct, fully spin polarized bands with the polarization directions parallel to the rotational symmetry axis,[26–35] an effect whose consequences were, to date, investigated theoretically mainly in quantum dot setups.[36–40] Recently the possibility of using gates to control the spin filtering properties due to SOI in CNT quantum dots has been also exploited.[41] While the band splitting properties of the SOI have been confirmed by experiments,[42–44] the spin-projective properties still require experimental testing.

In this paper, we show that single-wall CNT cross-junctions as shown in Fig. 1 are attractive candidates for further experimental progress for both spin-resolved transport and the detection of entanglement signatures. While such cross-junctions have already attracted much interest experimentally[45–51] and theoretically,[52–57] the novel features due to SOI have never been investigated before. Here we take the SOI fully into account, and consider setups with weak (usually sub-tesla)

magnetic fields **B** in the plane spanned by the two CNTs, often with **B** parallel to one of the CNTs.

We first demonstrate that close to the Dirac points the cross-junction operates as an efficient spin filter. Full spin polarization for an outgoing current is obtained if only one SOI-split subband contributes to the outgoing transport. This polarization can be reversed to opposite, yet not perfect polarization upon small changes of the gate potential such that further subbands become active for the transport. At fixed gate potential, however, a perfect reversal of the polarization in the lowest subband can be achieved by letting **B** → −**B**.

In the second part of this paper, we investigate the transport properties of entangled electron pairs passing through the cross-junction, as indicated by the hourglass shaped state in Fig. 1. We investigate the current noise correlators for signatures of the entanglement, notably for a bunching or antibunching behavior arising from the injection of singlet or triplet states. This investigation is an extension of previous work on semiconductor cross-junctions,[23,58] in which also SOI effects[59–61] were investigated. Due to the different band structure of CNTs and SOI effects, our results are quite different, and a comparison will be made accordingly below.

We will consider only cross-junctions of weakly coupled CNTs, allowing us to connect the scattering theory of the cross-junction directly to a microscopic Hamiltonian. Hence we do not treat high-efficiency (50-50) beam splitters such as required for proposed noise-measurement based proofs of entanglement through, for instance, Bell inequalities,[62–64] entanglement witnesses,[65] or quantum state tomography.[66] It should also be noted that a proof of entanglement does not necessarily need a beam splitter setup. If spin filters, for instance, as provided by the SOI-split CNT bands, are placed close to the source of entangled electron pairs, the current amplitude of the outgoing pairs is modulated by the nonlocal filter settings. Hence entanglement information can be obtained already from measuring currents only.[41]

The paper is organized as follows, in Sec. II we introduce the model for the CNT including the SOI effects, and we provide the scattering theory description of the cross-junction.
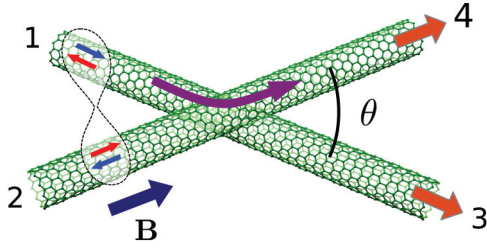
FIG. 1. (Color online) Two CNTs forming a cross-junction, a four-terminal system labeled by the leads $i = 1,2,3,4$ with a small contact area that allows electron tunneling between the CNTs, and an angle θ between the CNT axes. Any injected particle can at the junction either remain in the same CNT or tunnel into the other CNT, as illustrated by the bent arrow for the tunneling process $i = 1 \rightarrow i = 4$. We assume that particles are injected into leads $i = 1,2$ and their current is measured at the outgoing leads $i = 3,4$ (orange arrows). A magnetic field **B** is applied in the plane spanned by the two CNTs, and we mostly consider the case of **B** parallel to the nanotube with leads $i = 2,4$. This setup is explored for the combined effects of SOI and **B** on spin-filtered transport and signatures of entanglement from electron pairs, such as the incoming spin-entangled state indicated by the hourglass shape.

We then analyze in Sec. III the normal state cross-conductance and the spin filtering properties. In Secs. IV to VII we discuss the noise properties of injected entangled pairs. Section IV contains an analysis of different injection scenarios, Sec. V the proper analysis of the current noise correlators, Sec. VI the dependence of the noise on varying the external magnetic field, and Sec. VII a discussion of the noise properties under non-ideal particle injections. We conclude in Sec. VIII. Two appendices A and B contain some details of the calculations.

II. CNT CROSS-JUNCTIONS

A. CNT low-energy Hamiltonian

CNTs can be considered as graphene sheets that are rolled into a cylinder.[67] They inherit from graphene the low-energy band structure in the form of two Dirac valleys centered at momenta commonly denoted as K and K'. Since momenta are quantized in the transverse (circular) direction, the resulting CNT low-energy band structure consists of cuts through the Dirac cones, which form subbands labeled by the quantized transverse momenta $k_\perp$ and described by the single-particle Hamiltonian

$$H_0 = \hbar v_F (k_\perp \sigma_1 + k\tau \sigma_2), \tag{1}$$

where $\hbar$ is Planck's constant, $v_F \approx 0.9 \times 10^6$ m/s is the Fermi velocity, k are the longitudinal momenta along the CNT axis, $\tau = +,-=K,K'$ labels the Dirac valleys, and $\sigma_{1,2}$ are Pauli matrices referring to the A,B sublattice components of the wave functions. If the indices (N_1,N_2) denote the chirality of the CNT, i.e., how the graphene sheet is rolled together, we have $k_\perp = [n - (N_1 - N_2 \bmod 3)/3]/R$, with the integer n being the subband index, $R = a\sqrt{N_1^2 + N_2^2 + N_1 N_2}$ the CNT radius, and $a = 2.46$ Å the unit cell length.

The SOI and the hybridization of orbitals induced by the curvature of the surface of the CNT lead to additions to the Hamiltonian H_0 given by[29,30,32,33]

$$H_{cv} = \hbar v_F \left(\Delta k_\perp^{cv} \sigma_1 + \tau \Delta k_z^{cv} \sigma_2 \right), \tag{2}$$

$$H_{\text{SOI}} = (\alpha \sigma_1 + \tau \beta) S^z, \tag{3}$$

with S^z the Pauli matrix for the spin operator parallel to the CNT axis (all used Pauli matrices are normalized to eigenvalues ± 1), $\Delta k_{\perp,z}^{cv}$ the curvature induced momentum shifts, and α, β the SOI interaction strengths. The values of these parameters depend on the precise details of the elementary overlap integrals between the carbon orbitals and are subject to considerable uncertainty.[68–70] From a rather conservative estimate of the resulting SOI strength one obtains[32,33] $\hbar v_F \Delta k_\perp^{cv} = -\tau \cos(3\eta)5.4$ meV/$(R[\text{nm}])^2$, $\hbar v_F \Delta k_z^{cv} = \tau \sin(3\eta)5.4$ meV/$(R[\text{nm}])^2$, $\alpha = -0.08$ meV/$R[\text{nm}]$, and $\beta = -\cos(3\eta)0.31$ meV/$R[\text{nm}]$, for η the chiral angle defined by $\tan \eta = \sqrt{3}N_2/(2N_1 + N_2)$.

The application of an external magnetic field $\mathbf{B} = (B_x, B_y, B_z)$, with B_z parallel to the CNT axis, leads to the further terms

$$H_B = \mu_B g\mathbf{B} \cdot \mathbf{S} + |e|v_F R B_z \sigma_1/2, \tag{4}$$

incorporating the Zeeman effect and the Aharonov-Bohm flux of the magnetic field through the CNT cross section. Here $\mathbf{S} = (S^x, S^y, S^z)$ is the vector of spin Pauli matrices, μ_B the Bohr magneton, $g = 2$ the Landé g factor, and e the electron charge. We shall consider only weak fields not exceeding one or a few tesla, allowing us to neglect further orbital terms that would lead to the formation of Landau levels.

Figure 2 shows a typical spectrum resulting from the combination of SOI and the external magnetic field. The SOI spin-splits the bands and causes a spin S^z polarization along the CNT axis. Since the SOI maintains time-reversal symmetry, the bands in the K and K' valleys remain degenerate but
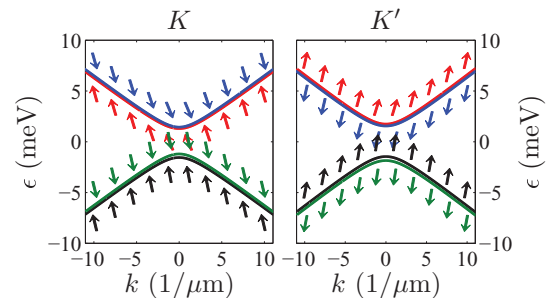

FIG. 2. (Color online) Lowest CNT bands close to the K and K' points for a CNT with chirality (30,12) in the presence of a magnetic field $|\mathbf{B}| = 0.6$ T at the angle $\theta = \pi/3$ with respect to the CNT axis. The combined effects of CNT curvature, SOI, and magnetic field fully gap the nominally metallic CNT and lead to entirely nondegenerate, fully spin polarized bands. The arrows next to the curves indicate the spin polarizations of the bands as a function of momentum k, in the plane spanned by $\mathbf{B}$ and the CNT axis (with the axis direction upwards in the plot). At large energies, the polarizations become energy independent and follow the effective, valley-dependent Zeeman fields $\mathbf{B}_\tau^{\text{eff}} = \tau \mathbf{B}_{\text{SOI}} + \mathbf{B}$. The shown SOI induced features are generic for all chiralities, except for armchair CNTs, including semiconducting CNTs, with the main difference being different SOI interaction strengths.

carry opposite spin polarizations. With the external magnetic field, the time-reversal symmetry is broken, and the effective Zeeman fields acting in both valleys are different. While for any momentum k each band remains fully spin polarized, the polarization directions are no longer opposite in the two valleys and the spins tend to align with the transversal component of the external field, as shown by the arrows in Fig. 2. We denote the corresponding (k,τ)-dependent spin eigenvalues by $\nu = \pm$.

Away from the Dirac points, the polarizations become k independent and the effective Zeeman field becomes $\mathbf{B}_{\tau,n}^{\mathrm{eff}} = \tau \mathbf{B}_{\mathrm{SOI},n} + \mathbf{B}$ with n the band index in each valley and $\mathbf{B}_{\mathrm{SOI},n}$ the result of the SOI in band n. In addition, the orbital effect of $\mathbf{B}$ shifts the energy levels such that both valleys also become energetically nondegenerate. In the low-energy regime close to the Dirac points, therefore, any transport is strongly subjected to the spin and valley filtering properties of the bands, together with a strongly enhanced density of states due to the curved band bottoms. Finally it should be noted that for $\mathbf{B}$ parallel to the CNT axis, S^z remains the good spin quantum number for all k, and ν is identified with the spin projection along the CNT axis.

B. Cross-junction

The cross-junctions considered in this paper act as scatterers transferring incoming electrons between the two nanotubes and between different bands within each nanotube. We describe these processes within the scattering matrix formalism,[71] for which the cross-junction forms a four-terminal system with two incoming $i = 1,2$ and two outgoing leads $i = 3,4$, as shown in Fig. 1. The scattering states are labeled by the further valley and spin quantum numbers τ, ν and the energies ϵ, and are represented by the states $|i,\tau,\nu,\epsilon\rangle$ and the fermion operators $a_{i\tau\nu}^{\dagger}(\epsilon)$.

We denote by $s_{(i,\tau,\nu),(i',\tau',\nu')}(\epsilon)$ the scattering matrix for the elastic process $|i',\tau',\nu',\epsilon\rangle \rightarrow |i,\tau,\nu,\epsilon\rangle$. We do not consider inelastic processes because the coherence length is usually larger than the typical dimension of the junction.

Two scenarios for the scattering matrix will be considered. First, we neglect backscattering between the incoming leads $i = 1,2$ and the outgoing leads $i = 3,4$.[58] In a basis for the leads $i = 1,2,3,4$, we then have

$$s = \begin{pmatrix} 0 & 0 & t_{1,3} & r_{1,4} \\ 0 & 0 & r_{2,3} & t_{2,4} \\ t_{3,1} & r_{3,2} & 0 & 0 \\ r_{4,1} & t_{4,2} & 0 & 0 \end{pmatrix}, \tag{5}$$

where $r_{i,i'}$ and $t_{i,i'}$ are matrices in τ,ν,ϵ. This description is appropriate for a larger contact area, and small θ in which the momentum of the incoming wave packets is approximately preserved.

Second, we focus on a contact area between the two CNTs with a linear extension much smaller than the size of typical incoming wave packets, which allows us to treat the tunnel junction as an elastic point contact scatterer. Such a situation is typically obtained when one CNT falls over another CNT.[46,50] Usually then the tunneling coupling is weak, allowing us to retain only first-order tunneling processes and exclude backscattering into the same lead. Scattering between leads $1 \leftrightarrow 2$ and $3 \leftrightarrow 4$, however, must now be taken into account.

The scattering matrix becomes

$$s = \begin{pmatrix} 0 & r_{1,2} & t_{1,3} & r_{1,4} \\ r_{2,1} & 0 & r_{2,3} & t_{2,4} \\ t_{3,1} & r_{3,2} & 0 & r_{3,4} \\ r_{4,1} & t_{4,2} & r_{4,3} & 0 \end{pmatrix}. \tag{6}$$

The consequences of both scenarios are discussed in Sec. V.

With the assumption of a weak tunneling amplitude, we proceed to make a Born approximation to link the scattering matrix to the microscopic tunneling Hamiltonian H_t. In this approximation, the tunneling between the two CNTs, the scattering between the leads $1 \leftrightarrow 4, 2 \leftrightarrow 3, 1 \leftrightarrow 2$, and $3 \leftrightarrow 4$ is expressed by

$$r_{(i,\tau,\nu),(i',\tau',\nu')}(\epsilon) = \langle i,\tau,\nu,\epsilon | H_t | i',\tau',\nu',\epsilon \rangle, \tag{7}$$

while the transmission within the same nanotube, $1 \leftrightarrow 3$ and $2 \leftrightarrow 4$, remains unperturbed

$$t_{(i,\tau,\nu),(i',\tau',\nu')}(\epsilon) = i\delta_{\tau,\tau'}\delta_{\nu,\nu'}. \tag{8}$$

Note that if we choose these matrix elements to be purely imaginary, we can choose real $r_{i,i'}$ below and maintain an approximate unitarity of the scattering matrix in the Born approximation. The tunneling can be described by a tight binding Hamiltonian of the form[53]

$$H_t = \sum_{\substack{\tau,\tau',\sigma,\sigma' \\ s,x_n,x_{n'}}} \lambda_{\tau,\sigma;\tau',\sigma'}(x_n,x_{n'})\tilde{a}_{2,\tau,\sigma,s}^{\dagger}(x_n)\tilde{a}_{1,\tau',\sigma',s}(x_{n'}) + \mathrm{H.c.},$$
$$\tag{9}$$

where $x_n, x_{n'}$ mark the unit cell positions of the two CNTs at the contact area, and $s = \uparrow, \downarrow$ denotes the spin projections in a global spin basis. The tunneling amplitudes $\lambda_{\tau,\sigma;\tau',\sigma'}(x_n,x_{n'})$ preserve the spin but may be sublattice and valley dependent. The operators $\tilde{a}_{i,\tau,\sigma,s}^{\dagger}$ are the microscopic electron operators, related to the scattering states by the transformation

$$a_{i,\tau,\nu}^{\dagger}(\epsilon) = \sum_{x_n,\sigma,s} g_{i,\tau,\nu,\epsilon}^{\sigma,s}(x_n)\tilde{a}_{i,\tau,\sigma,s}^{\dagger}(x_n), \tag{10}$$

with the transformation matrix g. It should be noted that while the valley τ is preserved, the sublattice, position, and global spin coordinates are summed out. Through the summation of the latter, together with the fact that H_t is spin preserving, the scattering matrix elements $r_{(i,\tau,\nu),(i',\tau',\nu')}$ are proportional to the spin overlap integral $\langle \nu | \nu' \rangle$ between the states ν and ν' of the two CNTs. If $\mathbf{S}_{i,\tau,\nu,\epsilon} = \langle i,\tau,\nu,\epsilon | \mathbf{S} | i,\tau,\nu,\epsilon \rangle$ is the spin polarization vector of band (i,τ,ν) at energy ϵ, this spin overlap integral allows us to express the scattering matrix elements for the tunneling processes as

$$|r_{(i,\tau,\nu),(i',\tau',\nu')}(\epsilon)|^2$$
$$= \Gamma \rho_{i,\tau,\nu,\epsilon} \rho_{i',\tau',\nu',\epsilon} (1 + \mathbf{S}_{i,\tau,\nu,\epsilon} \cdot \mathbf{S}_{i',\tau',\nu',\epsilon}), \tag{11}$$

with Γ the effective tunnel rate obtained from summing out the $\lambda_{\tau,\sigma;\tau',\sigma'}(x_n,x_{n'})$ in Eq. (9), and $\rho_{i,\tau,\nu,\epsilon}$ the density of states in band (i,τ,ν). It should be noted that close to a band bottom, at which one of the involved densities of states diverges, this perturbative formula is no longer accurate, and the singular behavior is truncated by higher order processes. However, since the bands are spin projective, the proportionality to $(1 + \mathbf{S}_{i,\tau,\nu,\epsilon} \cdot \mathbf{S}_{i',\tau',\nu',\epsilon})$ is maintained. As noted above, with the

choice of purely imaginary $t_{i,i'}$ we can set $r_{(i,\tau,\nu),(i',\tau',\nu')}(\epsilon) = \sqrt{|r_{(i,\tau,\nu),(i',\tau',\nu')}(\epsilon)|^2}$ and verify that any further sign in front of the square root does not have any influence on the results.

For energies ϵ largely exceeding the SOI energy scales, the scattering matrix tends to an energy-independent quantity, which we cover with the parameter R_∞ as

$$|r_{(i,\tau,\nu),(i',\tau',\nu')}(\epsilon)|^2 \sim \frac{R_\infty}{16}(1 + \mathbf{S}_{i,\tau,\nu} \cdot \mathbf{S}_{i',\tau',\nu'}). \quad (12)$$

Since $R_\infty \propto \Gamma$, we shall use the condition $R_\infty \ll 1$ to control the perturbative expansion.

Since the two CNTs cross at an angle θ, the spin directions ν and ν', which are further affected by the magnetic field, are generally not aligned. Therefore, the tunneling interface, although spin preserving, acts as a spin mixer within the *local* spin bases, with τ-dependent mixing amplitudes that are tunable through ϵ and the external magnetic field. This tunability causes the new features in the noise spectra reported in this paper.

It should finally be stressed that with the Born approximation the scattering matrix, Eq. (5), is no longer unitary, as unitarity imposes identities on inverse matrices and involves expansions to infinite order. For controlled perturbative expansions, therefore, the unitarity of the scattering matrix should be used with care.

III. NORMAL STATE CONDUCTANCE AND SPIN-FILTERING

The spin-filtering properties of the SOI on the cross-junction first become evident when considering the normal state cross-conductance. By the Landauer formula, the latter is given by

$$G_{\text{cross}}(\epsilon) = \frac{e^2}{h} \sum_{\tau,\tau',\nu,\nu'} R_{(4,\tau,\nu),(1,\tau',\nu')}(\epsilon), \quad (13)$$

with $R_{(4,\tau,\nu),(1,\tau',\nu')} = |r_{(4,\tau,\nu),(1,\tau',\nu')}|^2$. With the definition of R_∞ given in Eq. (12), we obtain in the large energy regime $G_{\text{cross}} \sim (e^2/h)R_\infty$. An example for this cross-conductance as a function of energy (bias) is shown in Fig. 3. As mentioned in the previous section, close to the gap the conductance is largely dominated by the strongly varying densities of states. This leads to the singular peaks in the figure, at which higher order processes would need to be taken into account. Yet even close to the peaks, the perturbative expansion remains well controlled. The peak structure indicates that progressively scattering channels are closed when approaching the gap. Since the SOI causes a spin filtering, this indicates also that the outgoing current can be spin polarized.

To make this evident, we choose the magnetic field parallel to the outgoing lead $i = 4$ (see Fig. 1), such that the eigenvalues $\nu = \pm$ coincide for all energies with the spin projections $\uparrow, \downarrow$ parallel to the CNT axis. The polarization of the outgoing current is then given by

$$p = \frac{\sum_{\tau,\tau',\nu'}[R_{(4,\tau,+),(1,\tau',\nu')} - R_{(4,\tau,-),(1,\tau',\nu')}]}{\sum_{\tau,\tau',\nu'}[R_{(4,\tau,+),(1,\tau',\nu')} + R_{(4,\tau,-),(1,\tau',\nu')}]}. \quad (14)$$

A typical result is represented in Fig. 4. If only one single scattering channel in the outgoing lead $i = 4$ is available,
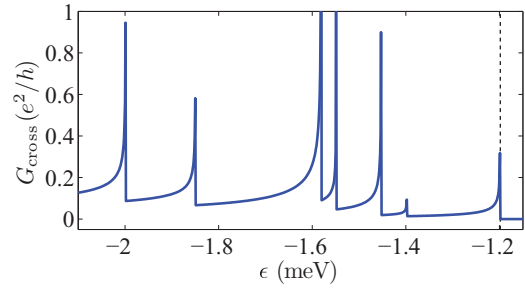

FIG. 3. (Color online) Cross-conductance G_{cross} for a cross-junction of two (30,12) CNTs at an angle $\theta = \pi/3$ in a magnetic field $B = 0.6$ T parallel to the outgoing lead $i = 4$. Displayed is a zoom on the valence band close to the Dirac points. The peaks indicate the van Hove singularities delimiting the various spin-polarized bands in both CNTs. These singularities are rounded off in the numerical implementation. The dashed vertical line marks the gap for the tunneling process (the larger gap of both CNTs; see the band structure in Fig. 2). The tunnel coupling between the CNTs is chosen such that $G_{\text{cross}} \to (e^2/h)R_\infty$ at large energies with $R_\infty = 0.05$.

full spin polarization is obtained. Yet quite remarkably, when crossing with the energy through a band bottom, the strongly enhanced density of states at the band bottom causes, within a fraction of a meV, a reversal of the polarization with a final amplitude that can exceed 80%. On the other hand, by reversing the magnetic field $\mathbf{B} \to -\mathbf{B}$, an energetically degenerate situation is obtained, yet with switched valleys and spins, such that the full polarization in the lowest band becomes a full polarization of opposite spin.

This use of the cross-junction as a versatile spin filter at high efficiency complements a previous suggestion of exploring bound states in SOI-split CNTs for perfect spin filtering.[34,72] It also complements the alternative of SOI induced spin-filtering in CNT quantum dot setups.[41]

IV. INJECTION OF ENTANGLED ELECTRON PAIRS

We now turn to the injection of spin-entangled electron pairs into the cross-junction, such as achieved by a Cooper
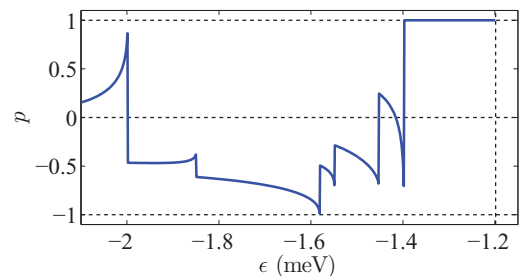

FIG. 4. (Color online) Spin polarization p for electrons in the outgoing lead $i = 4$ for the same conditions as in Fig. 3. Near the gap for the tunneling process (vertical dashed line), only one outgoing channel is available and the electrons are perfectly spin polarized. Small variations of the gate potential allow effective switching to the opposite spin direction with high (yet not perfect) efficiencies. A reversal of the magnetic field $\mathbf{B} \to -\mathbf{B}$ reversed all spin directions and can be used for perfect spin filtering of the opposite spin direction. The dashed horizontal lines are guides for the eye at $p = -1, 0, 1$.

pair splitter.[10–12] The spin-filtering characteristics of the CNTs require a careful analysis of how the electrons are injected into each CNT, and how they are transported to the cross-junction. Indeed, if the two CNTs are nonparallel at the injection region, a first nonparallel spin projection between both CNTs becomes effective already at injection and affects the entanglement. If the CNTs are strongly curved in the longitudinal direction, the eigenstates (τ, ν) of a straight CNT can hybridize and the entanglement information of the injected particles can get lost (see Fig. 5).

To minimize the latter effect, the energy scale associated with the longitudinal bending ϵ_{lb} must be smaller than the sub-meV scales due to the SOI.[73–76] Since the bending affects mainly the hopping integral between neighboring carbon ions, a rough estimate gives $\epsilon_{lb} \sim t R/r$ with $t \sim 3$ eV the hopping integral, R the CNT radius, and r the bending radius. A further reduction of this estimate by averaging over the CNT cross section can be expected. Since usually $R \sim 1$ nm, therefore, a bending radius larger than $r \sim 1$ μm is certainly required.

If such large enough radii can be maintained, the states arriving at the cross-junction correspond to the states at the injection region. Figure 5 shows different possible setups of connecting the CNTs to a superconducting entangler. In the following, we shall focus mainly on the situation of an *adiabatic* electron pair injection, in which the spin-correlation state arriving at the cross-junction in the *local* spin-eigenbasis ν bound to each CNT is identical to the state in the global spin-eigenbasis in the superconductor. Corresponding possible setups are shown in Figs. 5(a) and 5(b). We assume furthermore that both CNT branches between the entangler and the cross-junction are of comparable length, such that the wave packets of the injected particles strongly overlap at the cross-junction and the fermion statistics is of importance. We also focus on small injection rates such that the injected particles have a well defined energy spread.
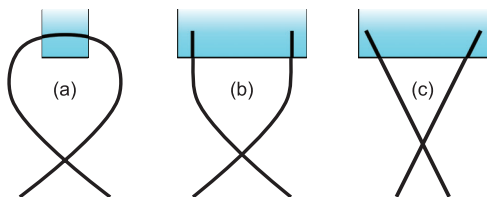

FIG. 5. (Color online) Possible scenarios for the connection of the CNTs (thick lines) to the entangler (boxes). If the entangler is a superconductor expelling the magnetic field in the parts of the CNTs it covers, the spin eigenstates in the CNT parts below the superconductor are parallel to the CNT axes. In situations (a) and (b) the spin eigenvalues in the left and right CNTs are then parallel. This allows for an *adiabatic* injection, in which any spin correlator of injected electron pairs remains identical in the *local* spin bases bound to the CNTs. After adiabatic transport to the cross-junction an injected spin singlet, for instance, arrives as a spin singlet in the local bases at the cross-junction. Situation (c) corresponds to a *nonadiabatic* injection, in which the local spin bases of the left and right CNT are nonparallel below the superconductor and the injected pair decomposes into $\nu = \pm$ eigenstates according to the angle between the two CNTs below the superconductor. This introduces a deterministic mixture of singlet and triplet states in the local spin bases at the cross-junction.

A *nonadiabatic* situation, in which the local spin bases at injection are nonparallel and a deterministic singlet-triplet mixture is obtained, is displayed in Fig. 5(c). Its consequences, as well as the consequences from nonoverlapping wave packets and a larger energy spread, are discussed in Sec. VII.

V. CURRENT NOISE

Information on the entanglement of the injected electron pairs can be drawn by measuring the current noise correlators of the cross-junction. Within the scattering matrix formalism, the current operator in lead i at time t takes the form[71]

$$I^i(t) = \frac{e}{h} \sum_{\substack{j,j',\tau_i,\tau,\tau' \\ \nu_i,\nu,\nu',\epsilon,\epsilon'}} A^{i,\tau_i,\nu_i}_{(j,\tau,\nu),(j',\tau',\nu')}(\epsilon,\epsilon')$$
$$\times a^\dagger_{j,\tau,\nu}(\epsilon) a_{j',\tau',\nu'}(\epsilon') e^{i(\epsilon-\epsilon')t/\hbar}, \quad (15)$$

with

$$A^{i,\tau_i,\nu_i}_{(j,\tau,\nu),(j',\tau',\nu')}(\epsilon,\epsilon') = \delta_{(i,\tau_i,\nu_i),(j,\tau,\nu)}\delta_{(i,\tau_i,\nu_i),(j',\tau',\nu')}\delta_{\epsilon,\epsilon'}$$
$$- s^*_{(i,\tau_i,\nu_i),(j,\tau,\nu)}(\epsilon)s_{(i,\tau_i,\nu_i),(j',\tau',\nu')}(\epsilon'). \quad (16)$$

Since we neglect backscattering into the same lead, the lead indices are restricted to outgoing leads $i = 3,4$ and incoming leads $j,j' = 1,2$, such that the Kronecker symbols in the latter equation drop out.

If $|\Psi\rangle$ is the state containing the injected particles, the symmetrized noise correlators for these current operators read

$$S^{ii'}(t) = \tfrac{1}{2}\langle\Psi|\{\delta I^i(t),\delta I^{i'}(0)\}|\Psi\rangle, \quad (17)$$

with $\delta I^i = I^i - \langle\Psi|I^i|\Psi\rangle$. The corresponding zero frequency ($\omega = 0$) noise is obtained by time averaging this quantity as

$$S^{ii'} = \lim_{\mathcal{T}\to\infty} \frac{h}{\mathcal{T}} \int_0^{\mathcal{T}} dt \, \mathrm{Re}\, S^{ii'}(t). \quad (18)$$

The evaluation of these correlators is carried out in Appendix A.

Let $|\Psi\rangle$ describe the injection of two particles, one in lead 1 and one in lead 2, in either a singlet state $|\Psi\rangle = |-\rangle$ or a spin-zero triplet state $|\Psi\rangle = |+\rangle$. If we assume an adiabatic injection as explained in Sec. IV, we have

$$|\pm\rangle = \sum_{\tau_1,\tau_2,\nu} (\nu)_\pm \, c_{\tau_1,\tau_2;\nu} \, a^\dagger_{2,\tau_2,\nu}(\epsilon_0)a^\dagger_{1,\tau_1,\bar\nu}(\epsilon_0)|0\rangle, \quad (19)$$

with $|0\rangle$ the equilibrium ground state (we assume temperature $T = 0$), and the pair of particles being injected with certainty into unoccupied states just above the Fermi surface, such that $\epsilon_0 \gtrsim \epsilon_F$, with ϵ_F the Fermi energy of the CNT. We use the convention $\bar\nu = -\nu$, and will use it below also for the valley indices, $\bar\tau = -\tau$. The symbol $(\nu)_\pm$ defines the signs $(+)_\pm = +$ and $(-)_\pm = \pm$, distinguishing between triplets and singlets. The wave function amplitudes $c_{\tau_1,\tau_2;\nu}$ are normalized to $\sum_{\tau_1,\tau_2,\nu}|c_{\tau_1,\tau_2;\nu}|^2 = 1$, where it should be noted that only those $c_{\tau_1,\tau_2;\nu}$ are nonzero for which any of the pairs of states $\{(1,\tau_1,\nu,\epsilon_0),(2,\tau_2,\bar\nu,\epsilon_0)\}$ or $\{(1,\tau_1,\bar\nu,\epsilon_0),(2,\tau_2,\nu,\epsilon_0)\}$ has a nonvanishing density of states. If both pairs exist, the amplitude is independent of ν to maintain the distinction between singlets and triplets, $c_{\tau_1,\tau_2;\nu} = c_{\tau_1,\tau_2}$.

In an ideal situation, the only constraint on the energy ϵ_0 is to be larger than ϵ_F. Realistically, however, a controlled injection of entangled electrons requires that ϵ_0 lies close to ϵ_F to minimize decay processes. Yet for optimal operation of the entangler, maintaining still an offset $\epsilon_0 - \epsilon_F$ may be favorable.[77] Exploring the ϵ_0 dependence of correlators, therefore, corresponds to tuning ϵ_F through the electron density in the CNTs, for instance, through a backgate, while maintaining a very small bias $\epsilon_0 - \epsilon_F$ for the pair injection.

From Eqs. (A11)–(A14) we obtain the following result for the cross-correlators over the states $|\pm\rangle$, assuming henceforth implicit summation over repeated indices (summation within the brackets for the last term),

$$
\begin{aligned}
S^{34}_{\pm} = {}& \frac{e^2}{2h} c^*_{\lambda_1, \lambda_2} c_{\lambda_1, \lambda_2} \left[A^3_{\lambda'_2, \gamma} A^4_{\gamma, \lambda_2} + A^4_{\lambda'_2, \gamma} A^3_{\gamma, \lambda_2} \right] \\
& + \frac{e^2}{2h} c^*_{\lambda'_1, \lambda_2} c_{\lambda_1, \lambda_2} \left[A^3_{\lambda'_1, \gamma} A^4_{\gamma, \lambda_1} + A^4_{\lambda'_1, \gamma} A^3_{\gamma, \lambda_1} \right] \\
& + \frac{e^2}{h} c^*_{\lambda'_1, \lambda_2} c_{\lambda_1, \lambda_2} \left[A^3_{\lambda'_2, \lambda_2} A^4_{\lambda'_1, \lambda_1} - A^3_{\lambda'_2, \lambda_1} A^4_{\lambda'_1, \lambda_2} \right] \\
& + \frac{e^2}{h} c^*_{\lambda'_1, \lambda_2} c_{\lambda_1, \lambda_2} \left[A^4_{\lambda'_2, \lambda_2} A^3_{\lambda'_1, \lambda_1} - A^4_{\lambda'_2, \lambda_1} A^3_{\lambda'_1, \lambda_2} \right]
\end{aligned}
$$

$$
\begin{aligned}
& - \frac{e^2}{h} \left[c^*_{\lambda'_1, \lambda_2} c_{\lambda_1, \lambda_2} A^3_{\lambda'_1, \lambda_1} + c^*_{\lambda_1, \lambda'_2} c_{\lambda_1, \lambda_2} A^3_{\lambda'_2, \lambda_2} \right] \\
& \times \left[c^*_{\lambda'_1, \lambda_2} c_{\lambda_1, \lambda_2} A^4_{\lambda'_1, \lambda_1} + c^*_{\lambda_1, \lambda'_2} c_{\lambda_1, \lambda_2} A^4_{\lambda'_2, \lambda_2} \right], \quad (20)
\end{aligned}
$$

where the $\lambda_i = (i, \tau_i, \nu_i)$, $\lambda'_i = (i, \tau'_i, \nu'_i)$ are labels bound to lead $i = 1, 2$, but $\gamma = (j, \tau, \nu)$ includes the unrestricted summation over $j = 1, \ldots, 4$. The wave functions are $c_{\lambda_1, \lambda_2} = (\nu_1)_\pm c_{\tau_1, \tau_2; \nu_1} \delta_{\nu_1, \bar{\nu}_2}$, and we have used the notation $A^3_{\lambda, \lambda'} = \sum_{\tau, \nu} A^{(3, \tau, \nu)}_{\lambda, \lambda'}(\epsilon_0, \epsilon_0)$.

The first two lines in Eq. (20) correspond to single-particle-like noise, expressed by the quantities C_1 and S_1 in Appendix A, which is independent of the type of entanglement between the two injected electrons. It turns out that at large energies ϵ_0 these terms vanish. The following two lines result from the full interference of both electrons at the junction and are sensitive to the entanglement and the fermion statistics. The last term expresses the subtraction of the uncorrelated background current from the product of the currents $\langle\pm|I^3|\pm\rangle\langle\pm|I^4|\pm\rangle$.

Using $A^3_{\lambda, \lambda'} = -\sum_{\tau, \nu} s^*_{(3, \tau, \nu), \lambda} s_{(3, \tau, \nu), \lambda'}$ and the Born approximation of the scattering matrix, the latter result becomes

$$
\begin{aligned}
S^{34}_{\pm} = {}& \frac{e^2}{h} \mathrm{Re} \Big\{ c^*_{\tau_1, \tau_2; \nu} c_{\tau'_1, \tau_2; \nu} \big[T_{3 \tau_1 \nu} r^*_{(4, \tau_4, \nu_4), (1, \tau_1, \nu)} r_{(4, \tau_4, \nu_4), (1, \tau'_1, \nu)} + t^*_{3, \tau_1, \nu} t^*_{4, \tau_4, \nu_4} r_{(3, \tau_1, \nu), (2, \tau_4, \nu_4)} r_{(4, \tau_4, \nu_4), (1, \tau'_1, \nu)} \big] \\
& + c^*_{\tau_1, \tau_2; \bar{\nu}} c_{\tau_1, \tau'_2; \bar{\nu}} \big[T_{4, \tau'_2, \nu} r^*_{(3, \tau_3, \nu_3), (2, \tau_2, \nu)} r_{(3, \tau_3, \nu_3), (2, \tau'_2, \nu)} + t^*_{3, \tau_3, \nu_3} t^*_{4, \tau_2, \nu_2} r_{(3, \tau_3, \nu_3), (2, \tau'_2, \nu)} r_{(4, \tau_2, \nu), (1, \tau_3, \nu_3)} \big] \Big\} \\
& + \frac{e^2}{h} \Big\{ |c_{\tau_1, \tau_2; \nu}|^2 T_{3, \tau_1, \nu} T_{4, \tau_2, \bar{\nu}} - 2 \mathrm{Re} \big[c^*_{\tau_1, \tau_2; \nu} c_{\tau'_1, \tau'_2; \nu'} t^*_{3, \tau_1, \nu} t^*_{4, \tau_2, \bar{\nu}} r_{(3, \tau_1, \nu), (2, \tau'_2, \bar{\nu}')} r_{(4, \tau_2, \bar{\nu}), (1, \tau'_1, \nu')} \big(\delta_{\nu, \nu'} \pm \delta_{\nu, \bar{\nu}'} \big) \big] \Big\} \\
& - \frac{e^2}{h} \Big\{ \big[|c_{\tau_1, \tau_2; \nu}|^2 T_{3, \tau_1, \nu} \big] \big[|c_{\tau_1, \tau_2; \nu}|^2 T_{4, \tau_2, \bar{\nu}} \big] + \big[|c_{\tau_1, \tau_2; \nu}|^2 T_{3, \tau_1, \nu} \big] \big[c^*_{\tau_1, \tau_2; \nu} c_{\tau'_1, \tau_2; \nu} r^*_{(4, \tau_4, \nu_4), (1, \tau_1, \nu)} r_{(4, \tau_4, \nu_4), (1, \tau'_1, \nu)} \big] \\
& + \big[|c_{\tau_1, \tau_2; \nu}|^2 T_{4, \tau_2, \bar{\nu}} \big] \big[c^*_{\tau_1, \tau_2; \nu} c_{\tau_1, \tau'_2; \nu} r^*_{(3, \tau_3, \nu_3), (2, \tau_2, \bar{\nu})} r_{(3, \tau_3, \nu_3), (2, \tau'_2, \bar{\nu})} \big] \Big\},
\end{aligned} \quad (21)
$$

where the order of terms is the same as in Eq. (20), and where we have used the notations $t_{3, \tau, \nu} = t_{(3, \tau, \nu), (1, \tau, \nu)}$, $t_{4, \tau, \nu} = t_{(4, \tau, \nu), (2, \tau, \nu)}$, $T_{3, \tau, \nu} = |t_{3, \tau, \nu}|^2$, and $T_{4, \tau, \nu} = |t_{4, \tau, \nu}|^2$. All parts of the scattering matrix are evaluated at the energy ϵ_0. For consistency with the Born approximation, we have neglected in the latter expression any term on the order of $|r|^4$.

We emphasize that this result for the cross-noise holds for both scattering matrices (5) and (6). For a scattering matrix of the form of Eq. (5) we furthermore have $S^{33} = -S^{34} = -S^{43} = S^{44}$ as a consequence of particle conservation, independently of the state $|\Psi\rangle$ (see Appendix B). Although the Born approximation violates the unitarity of the scattering matrix, we have checked by direct comparison of the approximate results that $S^{33}_{\pm} = -S^{34}_{\pm}$ is indeed maintained. For a scattering matrix of the form of Eq. (6), however, the latter equality no longer holds. Indeed, S^{33} acquires then an extra term involving the additional scattering between leads 3 and 4, such that

$$
\begin{aligned}
S^{33}_{\pm} = {}& -S^{34}_{\pm} + \frac{e^2}{h} c^*_{\tau_1, \tau_2; \nu} c_{\tau'_1, \tau_2; \nu} \\
& \times t^*_{3, \tau_1, \nu} t_{3, \tau'_1, \nu} r^*_{(3, \tau'_1, \nu), (4, \tau_4, \nu_4)} r_{(3, \tau_1, \nu), (4, \tau_4, \nu_4)}. \quad (22)
\end{aligned}
$$

This extra shift is independent of the entanglement and corresponds to a self-energy-like renormalization of the single-particle part of the noise correlators (adding to parts C_1 and S_1 in Appendix A). Since such a term tends to obscure the clean signatures of the entanglement, we will focus henceforth on the cross-correlators only.

Since from the unitarity of the scattering matrix it follows that $\langle I^3 \rangle = \langle\pm|I^3|\pm\rangle = e/h$ (not invoking any further Born approximation), the Fano factor $F^{34}_{\pm} = S^{34}_{\pm}/2e\langle I^3 \rangle$ is, up to a constant, the same as $S^{34}_{\pm}$. In Fig. 6 we plot $F^{34}_{\pm}$ as a function of the energy ϵ_0 of the injected particles. For comparison, we also show the Fano factor resulting from the incoherent injection of single particles, $F^{34}_{sp} = S^{34}_{sp}/2e\langle I^3 + I^4 \rangle = S^{34}_{sp}/(2e^2/h)$, obtained from $S^{34}_{sp}(t) = \sum_{i, \nu} \langle \Psi_{i, \nu} | \{\delta I^3(t), \delta I^4(0)\} | \Psi_{i, \nu} \rangle / 4$, for $i = 1, 2$ with $|\Psi_{i, \nu}\rangle = \frac{1}{\sqrt{2}} \sum_\tau a^\dagger_{i, \tau, \nu}(\epsilon_0)|0\rangle$. The corresponding expressions have been derived in Appendix A 3. Note the factor $1/2$ in F^{34}_{sp}, which causes an identical normalization as for $F^{34}_{\pm}$.

We observe in Fig. 6 that at large energies $|\epsilon_0|$ the signature of bunching and antibunching of a structureless conductor, $F^{34}_{+} \approx 0$ (yet see Sec. VI for B-field corrections) and $F^{34}_{-} \sim T R$ is recovered.[58] Close to the gap at the Dirac
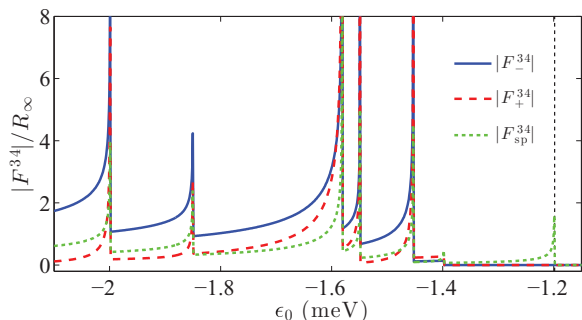
FIG. 6. (Color online) Fano factors for the triplet and singlet noise $F_{\pm}^{34}$ and the incoherent single-particle noise $F_{\rm sp}^{34}$ for the conditions as in Fig. 3, for the wave function $c_{\tau_1,\tau_2;\nu} \equiv c$, corresponding to an equal valley mixing of the injected particles, with $|c|^2 = 1/N$ for N the number of available scattering channels for injection [see the discussion following Eq. (19)]. As explained in the text, the dependence on ϵ_0 reflects usually a dependence on a backgate potential. The curves are normalized to $R_\infty = 0.05$ [see Eq. (12)]. The noise correlators show a similar peaked behavior as the conductance shown in Fig. 3. All curves are clearly distinct, yet their finer structure is better visualized through the modified Fano factors shown in Fig. 7. The dashed vertical line marks the gap for the tunnel junction.

points, however, the Fano factors are dominated by the strongly varying densities of states close to the band bottoms, similar to the behavior of the cross-conductance. A better resolution of the structure of the correlators close to the gap is therefore obtained by dividing the noise correlators by the normal state cross-conductance $G_{\rm cross}$, defining a modified Fano factor $\mathcal{F}^{34} = S^{34}/G_{\rm cross}$ with much suppressed singularities at the band bottoms. Figure 7 shows $\mathcal{F}_{\pm}^{34}$ and $\mathcal{F}_{\rm sp}^{34}$ as a function of energy.

This figure reveals some remarkable features resulting from the spin-filtering properties. We notice first that the gap for spin-correlated pairs is larger than for single-particle transport. Indeed, if we compare with the conductance in Fig. 3 and the polarization in Fig. 4 we notice that $\mathcal{F}_{\pm}^{34} = 0$ in the full range where $p = 1$, and transport is governed by a single outgoing channel in lead $i = 4$, while $\mathcal{F}_{\rm sp}^{34}$ remains nonzero. Even larger is the gap for the exchange part depending on the $\pm$ sign in the noise expressions, and we see that $S_{+}^{34} = S_{-}^{34}$ over a larger energy range. While for large energies $\mathcal{F}_{+}^{34} \approx 0$ (up to B-dependent corrections; see Sec. VI) and $\mathcal{F}_{-}^{34}$ exceeds the single-particle noise, the structure of the curves in the energy range dominated by the proximity to van Hove singularities strongly depends on the CNT chirality, the angle θ between the CNTs, and the magnetic field strength. However, for any choice of the latter values, a similar shape of the curves is obtained. We notice furthermore that the variations and jumps in the correlators $\mathcal{F}_{\pm}^{34}$ are more pronounced than those of $\mathcal{F}_{\rm sp}^{34}$, which remains always close to $\mathcal{F}_{\rm sp}^{34} \approx 0.5$. This behavior is closely connected to the large jumps in polarization p upon varying ϵ_0 (see Fig. 4), which affects a spin-correlated state much more than an incoherently spin-averaged single-particle state. It should also be noted that the value $\mathcal{F}_{\rm sp}^{34} \approx 0.5$ results from the spin averaging procedure and the chosen normalization of $\mathcal{F}_{\rm sp}^{34}$.
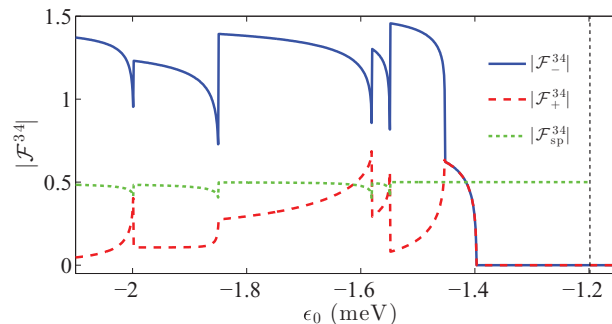

FIG. 7. (Color online) Modified Fano factors $\mathcal{F}_{\pm}^{34}$ and $\mathcal{F}_{\rm sp}^{34}$ corresponding to the curves shown in Fig. 6. The dominating peak structure by the van Hove singularities is largely suppressed. Notable distinctions between the triplet, singlet, and uncorrelated single-particle noise correlators are: (a) Correlated spin-zero particle pairs have a larger gap in the transport than single particles (vertical dashed line) as a result of the spin filtering. (b) The asymptotics represent the bunching–antibunching behavior with vanishing triplet noise $\mathcal{F}_{+}^{34} \to 0$ and a singlet noise $\mathcal{F}_{-}^{34}$ exceeding the single-particle noise $\mathcal{F}_{\rm sp}^{34}$. (c) The structure between the gap and the asymptotics is nonuniversal, depending on chirality, θ, and $\mathbf{B}$, yet is similar for any CNT. The spin filtering effect causes larger variations of the curves for spin-correlated electrons than for the uncorrelated single-particle noise (the value $\mathcal{F}_{\rm sp}^{34} \approx 0.5$ is a consequence of the normalization and the averaging of this noise).

VI. MAGNETIC FIELD DEPENDENCE

At energies $|\epsilon|$ far away from all the SOI induced gaps, the spin polarizations of the various bands become constants, parallel to the effective valley-dependent fields $\mathbf{B}_{\tau}^{\rm eff} = \tau \mathbf{B}_{\rm SOI} + \mathbf{B}$ (we restrict to the lowest band and drop the band index n). Since furthermore the densities of states tend to a constant, we see from Eq. (11) that the tunneling matrix elements become

$$|r_{(i,\tau,\nu),(i',\tau',\nu')}|^2 \to R\frac{1 + \mathbf{S}_{i,\tau,\nu} \cdot \mathbf{S}_{i',\tau',\nu'}}{2}, \qquad (23)$$

with, for convenience, $R = R_\infty/16$ [see Eq. (12)] and spin polarizations independent of ϵ.

To facilitate the discussion, we assume that the magnetic field is applied parallel to CNT 2 (leads $i = 2,4$, see Fig. 1), such that $\mathbf{B}_{\tau}^{\rm eff}$ is parallel to $\mathbf{B}$ in this CNT, and makes an angle θ_τ with the other CNT (leads $i = 1,3$), given by

$$\tan(\theta_\tau) = \frac{\tau B_{\rm SOI}\sin(\theta)}{B + \tau B_{\rm SOI}\cos(\theta)}, \qquad (24)$$

with θ the angle between the CNTs, $B_{\rm SOI} = |\mathbf{B}_{\rm SOI}|$, and $B = |\mathbf{B}|$. Consequently

$$|r_{(3,\tau,\pm),(2,\tau',\pm)}|^2 \to R\frac{1 + \cos(\theta_\tau)}{2} = R\cos^2(\theta_\tau/2), \quad (25)$$

$$|r_{(3,\tau,\pm),(2,\tau',\mp)}|^2 \to R\frac{1 + \sin(\theta_\tau)}{2} = R\sin^2(\theta_\tau/2). \quad (26)$$

For CNTs with radii of ~ 1 nm, we find that $B_{\rm SOI} \gtrsim 1$ T. For external fields up to the tesla range, we then can expand the noise correlators as a function of $B/B_{\rm SOI} < 1$. With

$|t_{(j,\tau,\nu),(1,\tau,\nu)}|^2 \rightarrow T$ for $j = 3, 4$ we obtain from Eq. (21)

$$S_{\pm}^{34} = -\frac{e^2}{h} 2 T R \left\{ c_{\tau_1,\tau_2;\nu}^* c_{\tau_1',\tau_2;\nu} + c_{\tau_1,\tau_2;\nu}^* c_{\tau_1,\tau_2';\nu} \right.$$
$$- c_{\tau_1,\tau_2;\nu}^* c_{\tau_1',\tau_2';\nu'} \left[\delta_{\nu,\nu'} \sin^2 \frac{\theta}{2} \pm \delta_{\nu,\bar{\nu}'} \cos^2 \frac{\theta}{2} \right] \right\}$$
$$+ \frac{e^2}{h} T R \frac{\sin^2 \theta \, B^2}{2 B_{\text{SOI}}^2} \left\{ 2 c_{\tau_1,\tau_2;\nu}^* c_{\bar{\tau}_1,\tau_2;\nu} \right.$$
$$+ c_{\tau_1,\tau_2;\nu}^* c_{\tau_1,\tau_2';\nu'} 3 \cos\theta [\delta_{\nu,\nu'} \mp \delta_{\nu,\bar{\nu}'}]$$
$$+ c_{\tau_1,\tau_2;\nu}^* c_{\bar{\tau}_1,\tau_2';\nu'} [\delta_{\nu,\nu'}(2\cos\theta - 1) \mp \delta_{\nu,\bar{\nu}'}(2\cos\theta + 1)] \right\}. \tag{27}$$

If a valley-independent injection is assumed, $c_{\tau_1,\tau_2;\nu} = 1/\sqrt{8}$, this expansion becomes more transparent. Resolving it explicitly for triplet and singlet injection we have, up to quadratic order in B,

$$S_+^{34} \sim -\frac{e^2}{h} T R \frac{\sin^2(\theta) B^2}{B_{\text{SOI}}^2}, \tag{28}$$

$$S_-^{34} \sim -\frac{e^2}{h} T R \left\{ 16 \cos^2(\theta/2) - \frac{\sin^2(\theta) B^2}{B_{\text{SOI}}^2} [1 + 10\cos(\theta)] \right\}. \tag{29}$$

Let us consider first the result at $B = 0$. The factor 16 in S_-^{34} is proportional to the number of scattering channels and must be compared with the result $S_-^{34} = (e^2/h) 4 T R$ for the single-channel case.[58] Moreover we note the angular dependence on $\cos^2(\theta/2)$ for the singlet case as a consequence of the spin projections during the tunneling process.

A similar angular dependence is obtained from the SOI in semiconductor beam splitters.[60] Yet in the latter the angle originates from the precession of the spins when traveling through a SOI region before reaching the beam splitter and as such is tunable by side gates, while for the CNTs it is a consequence of the crossing angle at the junction and the projective nature of the SOI and is fixed.

The main tunability in CNTs arises from the magnetic field dependence. At nonzero but small B, the first B-field corrections are quadratic in B/B_{SOI}. Remarkably, they have opposite signs for singlet and triplet cases, with the triplet increasing from 0 and the singlet decreasing from its $B = 0$ value. This behavior should be further compared with the B-field dependence of single particle noise. From the results of Appendix A 3 we obtain the expansions, up to order B^2, when injecting any spin ν into lead $i = 1, 2$, with equal amplitudes in both valleys τ,

$$S_{\text{sp},i=1}^{34} \sim -\frac{e^2}{h} T R \left[4 - \frac{\sin^2(\theta) B^2}{2 B_{\text{SOI}}^2} \right], \tag{30}$$

$$S_{\text{sp},i=2}^{34} \sim -\frac{e^2}{h} 4 T R. \tag{31}$$

We note that for particles injected into lead $i = 2$ the noise correlators are independent of the magnetic field for a scattering matrix of the form of Eq. (23), yet a weak dependence can remain through the field dependence of the densities of states. On the other hand, the B^2 dependence of the noise correlators for injection into lead $i = 1$ is similar to the singlet case. Yet for the incoherently averaged single-particle injection $S_{\text{sp}}^{34} = (S_{\text{sp},1}^{34} + S_{\text{sp},2}^{34})/2$ the overall amplitude
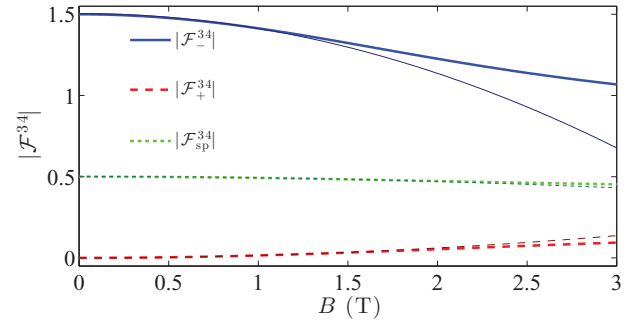

FIG. 8. (Color online) Magnetic field dependence of the modified Fano factors for the (30,12) CNT cross-junction with $\theta = \pi/3$ as for Fig. 3. The energy is fixed at $\epsilon = -30$ meV. The thick curves display the full expressions for $\mathcal{F}_{\pm}^{34}$ and $\mathcal{F}_{\text{sp}}^{34}$. The thinner, darker lines show the corresponding expansions to order B^2/B_{SOI}^2.

of the B^2-dependent terms is much reduced compared with S_-^{34}. This behavior is visible in Fig. 8, in which we display the B-field dependence of $\mathcal{F}_{\pm}^{34}$ and $\mathcal{F}_{\text{sp}}^{34}$.

VII. INFLUENCE OF DEVIATIONS FROM ADIABATIC INJECTION

In a realistic implementation, the previous result can be affected by several effects that we discuss in the following. Such effects generally perturb the clean entanglement signatures, and we provide here estimates of their influence.

Nonadiabatic pair injection. In the case of a nonadiabatic spin injection, the electron pair decomposes in nonparallel local spin eigenstates at the injection. As a consequence, the local triplet and singlet states $|\pm\rangle$ have further "local-spin-1" wave function components $|\pm, \pm\rangle \propto a_{1,\tau,\pm}^\dagger a_{2,\tau,\pm}^\dagger |0\rangle$. If the injection is spin independent, however, there is no mixing between the local $|\pm\rangle$ states. All averages between any of these wave function components are generally nonzero, and all the further contributions have a similar form as Eqs. (20) and (21), with the effect of washing out the derived distinctions between the singlet and triplet states. To gauge the amplitude of this perturbation, let θ_{na} be the angle between the spin eigenaxes at injection ($\theta_{na} = 0$ for adiabatic injection). This angle plays a similar role as θ for the cross-junction and, for instance, for a situation as in Fig. 5(c), $\theta_{na} = \theta$. Hence the previously derived correlators are weighted by $\cos^2 \theta_{na}$, and the further terms have amplitudes proportional to $\sin\theta_{na}\cos\theta_{na}$ and $\sin^2\theta_{na}$. For clear entanglement signatures, therefore, $\tan\theta_{na}$ should be kept small.

Same lead injection. In any setup, a part of the injected pairs does not split but enters the same lead. In a CNT, the Pauli principle is a weaker inhibitor for same-lead injection than in semiconductor wires, because of the further valley quantum state τ, allowing even an equal energy injection. This favors the transfer of spin entanglement onto an orbital entanglement, and again the resulting correlators have a similar shape as for the split pairs. However, since two particles are transmitted within the same CNT, the overall amplitude is proportional to the square of the transmission amplitude, $\sim T^2$, and therefore is much larger. Such contributions produce a large background on the noise from split electron pairs,

which should be detectable and may be subtracted from the measurement data. High splitting efficiencies generally require further interaction effects such as the Coulomb blockade.[11,12]

Different arrival times. If the two branches of the CNTs between injection points and the cross-junction are of different length, such that at arrival the wave packets of the two injected particles do not overlap, the bunching and antibunching behavior is suppressed. This corresponds to the case in which the terms C_2 and S_2 in Eqs. (A9) and (A14) vanish. The averaged noise then maintains some information on the spin correlations, but the information on the entanglement arising from the exchange part of the correlators proportional to the $\pm$ signs is lost.

Energy spread of the injected wave packets. It was assumed in the calculation that the energy levels of the injected particles are fixed to ϵ_0. This requires the limit of low temperatures T and small tunnel rates for the injection Γ_{inj}, such that $k_B T, \Gamma_{inj} < \Delta\epsilon$, with $\Delta\epsilon$ the level spacing of the CNTs. While maintaining $k_B T < \Delta\epsilon$ is desirable to avoid covering the signal behind the thermal noise $\sim T$, the smallness of Γ_{inj} is less critical if the scattering at the cross-junction is elastic. In this case, all displayed curves are just smeared out over energy windows of the width Γ_{inj}, centered about the values ϵ_0. This is different from a mesoscopic beam splitter that allows for inelastic processes, for which $\Gamma_{inj} > \Delta\epsilon$ has a larger impact.[60]

Valley-selective tunneling. In the shown figures for the noise correlators we have considered wave function amplitudes $c_{\tau_1,\tau_2;\nu} \equiv c$ that contained an equal distribution of the injected electron over the two valleys. Such an equal distribution is obtained when the tunneling into the CNTs is mostly local. Different contacts, however, are perfectly possible: for instance, some specific τ bound injection into a CNT, or the situation in which the opposite momenta of Cooper pairs in the superconductor are maintained in the form of tunneling into opposite valleys $(i = 1, \tau)$ and $(i = 2, \bar{\tau})$ only. Such situations impose further constraints on the correlators, and overall just reduce their amplitude, yet do not affect them qualitatively. More subtle is the case in which the wave functions in different valleys pick up different (deterministic or random) phases during transport to the cross-junction. This leads to an orbital interference effect that competes with the singlet–triplet signatures, and as a general rule produces correlators that lie somewhere between the singlet and triplet results.

VIII. CONCLUSIONS

In this paper we have shown that CNT cross-junctions have rich and tunable spin-dependent properties due to the SOI. First, this turns such cross-junctions into versatile spin filters, allowing generically to obtain perfect spin polarizations at low energies. By reversing the magnetic field $\mathbf{B} \rightarrow -\mathbf{B}$, the polarization is reversed as well. Opposite polarizations that can exceed 80% are also achievable by small changes of the backgate potential.

Second, the SOI adds further possibilities to obtain information on the entanglement of injected pairs of spins. In particular, it strongly affects the bunching and antibunching behavior of injected singlet and triplet states. At energies in which the number of scattering channels is reduced, the spin projective properties allow us to distinguish between spin

correlated and spin uncorrelated pairs, notably with correlated pairs of opposite spin having a larger gap in transport. At larger energies, at which the densities of state become constant, the spin exchange parts of the noise correlators acquire a dependence on θ similar to the dependence on the SOI-angle in the semiconductor setup described in Ref. 60. However, for the CNTs the angle θ, which is the crossing angle of the junction, is not tunable, in contrast to the semiconductor case. Tunable instead is the magnetic field $\mathbf{B}$, and we have shown that singlet and triplet correlations lead to a qualitatively different $\mathbf{B}$ dependence, clearly distinct from the dependence of noise of uncorrelated particles.

The described effects are pronounced in all types of CNTs, with the exception of armchair CNTs which do not have the gap induced by SOI and curvature.

To conclude we note that the use of ferromagnetic contacts on the outgoing leads could provide further indicators for entanglement. Indeed, the most sensitive part of the noise correlators to magnetic filtering are the exchange terms distinguishing between singlets and triplets. By rotating, for instance, the magnetization direction of the contacts through various angles, we expect therefore a modulation of the noise correlators with opposite sign for the singlet and triplet cases, on top of the behavior investigated in this paper. A systematic study of this effect is left for future work.

APPENDIX A: EVALUATION OF THE CORRELATORS

1. General form of correlators

The noise correlators are obtained by evaluating expectation values of the general form

$$C(t) = e^{i(\epsilon_\gamma - \epsilon_{\gamma'})t/\hbar} \langle \lambda_1, \lambda_2 | a_\gamma^\dagger a_{\gamma'} a_\delta^\dagger a_{\delta'} | \lambda_1', \lambda_2' \rangle, \quad (A1)$$

with the labels $\lambda, \gamma, \ldots$ covering all internal quantum states for the scattering states, including leads, valleys, and spin eigenstates, and where we have used $a_\gamma(t) = e^{-i\epsilon_\gamma t/\hbar} a_\gamma$. The time averaging done by a measurement is expressed by the integral

$$C = \frac{h}{\mathcal{T}} \int_0^{\mathcal{T}} dt \, \mathrm{Re} \, C(t) = \frac{h}{2\mathcal{T}} \int_{-\mathcal{T}}^{\mathcal{T}} dt \, C(t), \quad (A2)$$

in which we let $\mathcal{T} \rightarrow \infty$. Through the normalization by the Planck constant h the resulting noise has the dimension of e^2/h. Since the only time-dependent quantity in $C(t)$ is the phase factor, the time averaging gives a factor $\delta_{\epsilon_\gamma, \epsilon_{\gamma'}}$, such that

$$C = h \delta_{\epsilon_\gamma, \epsilon_{\gamma'}} \langle \lambda_1, \lambda_2 | a_\gamma^\dagger a_{\gamma'} a_\delta^\dagger a_{\delta'} | \lambda_1', \lambda_2' \rangle, \quad (A3)$$

By Wick's theorem we can write $C = h \delta_{\epsilon_\gamma, \epsilon_{\gamma'}} \sum_{n=0}^2 C_n$, where n denotes the number of contractions between the operators of the injected particles $\lambda_{1,2}$ and the operators related to the

current operator, $\gamma,\gamma',\delta,\delta'$. Since $|\lambda_1,\lambda_2\rangle = a^\dagger_{\lambda_1}a^\dagger_{\lambda_2}|0\rangle$, we have

$$C_0 = \left(\delta_{\lambda_1,\lambda'_1}\delta_{\lambda_2,\lambda'_2} + \delta_{\lambda_1,\lambda'_2}\delta_{\lambda_2,\lambda'_1}\right)\langle 0|a^\dagger_\gamma a_{\gamma'}a^\dagger_\delta a_{\delta'}|0\rangle, \quad \text{(A4)}$$

in which the remaining average corresponds to the usual noise at thermal equilibrium. In the low-temperature limit $k_B T < \Delta\epsilon$, with $\Delta\epsilon$ the level spacing, these contributions vanish. Indeed,

$$\langle 0|a^\dagger_\gamma a_{\gamma'}a^\dagger_\delta a_{\delta'}|0\rangle$$
$$= \delta_{\gamma,\gamma'}\delta_{\delta,\delta'}f(\epsilon_\gamma)f(\epsilon_\delta) + \delta_{\gamma,\delta'}\delta_{\delta,\gamma'}[1 - f(\epsilon_\gamma)]f(\epsilon_\delta), \quad \text{(A5)}$$

where $f(\epsilon)$ is the Fermi function. The first term corresponds to product of current averages and eventually will be subtracted in the noise correlators. For elastic processes we have $\epsilon_\gamma = \epsilon_\delta$ and the second term vanishes because $f(\epsilon_\gamma)[1 - f(\epsilon_\gamma)] = 0$ at low temperatures for discrete levels. For $k_B T > \Delta\epsilon$, it would produce the usual $\sim T$ dependence of thermal noise.

Since the injected particles are placed above the Fermi surface with certainty, their contractions are not weighted by the Fermi distribution and are equal to 1. Therefore, the contribution including one contraction with the injected particles is

$$\begin{aligned} C_1 &= \delta_{\lambda_1,\lambda'_1}\langle\lambda_2|a^\dagger_\gamma a_{\gamma'}a^\dagger_\delta a_{\delta'}|\lambda'_2\rangle_{\text{conn}} \\ &+ \delta_{\lambda_1,\lambda'_2}\langle\lambda_2|a^\dagger_\gamma a_{\gamma'}a^\dagger_\delta a_{\delta'}|\lambda'_1\rangle_{\text{conn}} \\ &+ \delta_{\lambda_2,\lambda'_1}\langle\lambda_1|a^\dagger_\gamma a_{\gamma'}a^\dagger_\delta a_{\delta'}|\lambda'_2\rangle_{\text{conn}} \\ &+ \delta_{\lambda_2,\lambda'_2}\langle\lambda_1|a^\dagger_\gamma a_{\gamma'}a^\dagger_\delta a_{\delta'}|\lambda'_1\rangle_{\text{conn}}, \end{aligned} \quad \text{(A6)}$$

in which the fully connected correlators of a single injected particle are given by

$$\begin{aligned} &\langle\lambda|a^\dagger_\gamma a_{\gamma'}a^\dagger_\delta a_{\delta'}|\lambda'\rangle_{\text{conn}} \\ &= \overbracket{a_\lambda a^\dagger_\gamma}\,\overbracket{a_{\gamma'}a^\dagger_\delta}\,\overbracket{a_{\delta'}a^\dagger_{\lambda'}} + \overbracket{a_\lambda a^\dagger_\gamma}\,a_{\gamma'}\overbracket{a^\dagger_\delta a_{\delta'}}a^\dagger_{\lambda'} \\ &+ \overbracket{a_\lambda a^\dagger_\gamma a_{\gamma'}a^\dagger_\delta}\,\overbracket{a_{\delta'}a^\dagger_{\lambda'}} + \overbracket{a_\lambda a^\dagger_\gamma a_{\gamma'}a^\dagger_\delta a_{\delta'}a^\dagger_{\lambda'}} \\ &= \delta_{\lambda,\gamma}\delta_{\gamma',\delta}\delta_{\delta',\lambda'}[1 - f(\epsilon_\gamma)] + \delta_{\lambda,\gamma}\delta_{\gamma',\lambda'}\delta_{\delta',\delta}f(\epsilon_\delta) \\ &+ \delta_{\lambda,\delta}\delta_{\gamma',\gamma}\delta_{\delta',\lambda'}f(\epsilon_\gamma) - \delta_{\lambda,\delta}\delta_{\gamma',\lambda'}\delta_{\delta',\gamma}f(\epsilon_\delta). \quad \text{(A7)} \end{aligned}$$

Since low temperatures $k_B T < \Delta\epsilon$ and elastic scattering are considered, all the Fermi functions in the latter equation vanish, as their energy is pinned to the energy of the injected particles above the Fermi surface. The remaining term gives the result

$$\langle\lambda|a^\dagger_\gamma a_{\gamma'}a^\dagger_\delta a_{\delta'}|\lambda'\rangle_{\text{conn}} = \delta_{\lambda,\gamma}\delta_{\gamma',\delta}\delta_{\delta',\lambda'}. \quad \text{(A8)}$$

Finally, the fully contracted part reads

$$\begin{aligned} C_2 &= \overbracket{a_{\lambda_2}a_{\lambda_1}a^\dagger_\gamma a_{\gamma'}a^\dagger_\delta a_{\delta'}a^\dagger_{\lambda'_1}a^\dagger_{\lambda'_2}} + \overbracket{a_{\lambda_2}a_{\lambda_1}a^\dagger_\gamma a_{\gamma'}a^\dagger_\delta a_{\delta'}a^\dagger_{\lambda'_1}a^\dagger_{\lambda'_2}} \\ &+ \overbracket{a_{\lambda_2}a_{\lambda_1}a^\dagger_\gamma a_{\gamma'}a^\dagger_\delta a_{\delta'}a^\dagger_{\lambda'_1}a^\dagger_{\lambda'_2}} + \overbracket{a_{\lambda_2}a_{\lambda_1}a^\dagger_\gamma a_{\gamma'}a^\dagger_\delta a_{\delta'}a^\dagger_{\lambda'_1}a^\dagger_{\lambda'_2}} \\ &= \delta_{\lambda_1,\gamma}\delta_{\lambda_2,\delta}\delta_{\lambda'_1,\gamma'}\delta_{\lambda'_2,\delta'} - \delta_{\lambda_1,\delta}\delta_{\lambda_2,\gamma}\delta_{\lambda'_1,\gamma'}\delta_{\lambda'_2,\delta'} \\ &+ \delta_{\lambda_1,\delta}\delta_{\lambda_2,\gamma}\delta_{\lambda'_1,\delta'}\delta_{\lambda'_2,\gamma'} - \delta_{\lambda_1,\gamma}\delta_{\lambda_2,\delta}\delta_{\lambda'_1,\delta'}\delta_{\lambda'_2,\gamma'}. \quad \text{(A9)} \end{aligned}$$

By a similar investigation we obtain the expectation values for the current operator,

$$\begin{aligned} I &= \langle\lambda_1,\lambda_2|a^\dagger_\gamma a_{\gamma'}|\lambda'_1,\lambda'_2\rangle \\ &= I_{eq} + \delta_{\lambda_1,\lambda'_1}\delta_{\lambda_2,\gamma}\delta_{\gamma',\lambda'_2} + \delta_{\lambda_1,\lambda'_2}\delta_{\lambda_2,\gamma}\delta_{\gamma',\lambda'_1} \\ &+ \delta_{\lambda_2,\lambda'_1}\delta_{\lambda_1,\gamma}\delta_{\gamma',\lambda'_2} + \delta_{\lambda_2,\lambda'_2}\delta_{\lambda_1,\gamma}\delta_{\gamma',\lambda'_1}, \quad \text{(A10)} \end{aligned}$$

where I_{eq} contributes to the background current that is independent of the injected particles and vanishes in the zero-bias, low-temperature limit considered here.

2. Pair injection in two leads

The situation of injecting each particle in a different CNT is expressed by a wave function $|\Psi\rangle = \sum_{\lambda_1,\lambda_2} c_{\lambda_1,\lambda_2}|\lambda_1,\lambda_2\rangle$ with λ_i restricted to lead $i = 1,2$ and c_{λ_1,λ_2} the wave function amplitudes. From the latter results, the current in lead j is

$$\begin{aligned} \langle I^j\rangle &= \langle\Psi|I^j|\Psi\rangle = \frac{e}{h}\sum_{\lambda_1,\lambda'_1,\lambda_2}c^*_{\lambda_1,\lambda_2}c_{\lambda'_1,\lambda_2}A^j_{\lambda_1,\lambda'_1} \\ &+ \frac{e}{h}\sum_{\lambda_1,\lambda_2,\lambda'_2}c^*_{\lambda_1,\lambda_2}c_{\lambda_1,\lambda'_2}A^j_{\lambda_2,\lambda'_2}, \quad \text{(A11)} \end{aligned}$$

with $A^j_{\lambda,\lambda'} = \sum_{\tau,\nu}A^{j,\tau,\nu}_{\lambda,\lambda'}$. The noise correlators, on the other hand, are

$$S^{jj'} = \frac{1}{2}\langle\Psi|\{\delta I^j,\delta I^{j'}\}|\Psi\rangle = \frac{e^2}{h}(S_1 + S_2) - h\langle I^j\rangle\langle I^{j'}\rangle, \quad \text{(A12)}$$

with

$$\begin{aligned} S_1 &= \frac{1}{2}\sum_{\lambda_1,\lambda_2,\lambda'_2,\gamma}c^*_{\lambda_1,\lambda_2}c_{\lambda_1,\lambda'_2}\left[A^j_{\lambda_2,\gamma}A^{j'}_{\gamma,\lambda'_2} + A^{j'}_{\lambda_2,\gamma}A^j_{\gamma,\lambda'_2}\right] \\ &+ \frac{1}{2}\sum_{\lambda_1,\lambda'_1,\lambda_2,\gamma}c^*_{\lambda_1,\lambda_2}c_{\lambda'_1,\lambda_2}\left[A^j_{\lambda_1,\gamma}A^{j'}_{\gamma,\lambda'_1} + A^{j'}_{\lambda_1,\gamma}A^j_{\gamma,\lambda'_1}\right], \end{aligned} \quad \text{(A13)}$$

and

$$\begin{aligned} S_2 &= \sum_{\lambda_1,\lambda'_1,\lambda_2,\lambda'_2}c^*_{\lambda_1,\lambda_2}c_{\lambda'_1,\lambda'_2}\left[A^j_{\lambda_2,\lambda'_2}A^{j'}_{\lambda_1,\lambda'_1} - A^j_{\lambda_2,\lambda'_1}A^{j'}_{\lambda_1,\lambda'_2}\right] \\ &+ (j \leftrightarrow j'). \quad \text{(A14)} \end{aligned}$$

3. Single-particle injection

The noise of a single particle that is injected into lead $i = 1,2$ is determined by averaging over the wave function $|\Psi_i\rangle = \sum_{\tau,\nu}c_{i,\tau,\nu}a^\dagger_{i,\tau,\nu}(\epsilon_0)|0\rangle$, for $\sum_{\tau,\nu}|c_{i,\tau,\nu}|^2 = 1$. The noise correlators for this state are straightforwardly obtained from the previous results by setting $C_2 = 0$ and by retaining only the term proportional to $\langle\lambda'_i|\dots|\lambda_i\rangle$ in C_1. It follows that

$$\begin{aligned} S^{jj'}_{\text{sp},i} &= \frac{e^2}{2h}\sum_{\lambda_i,\lambda'_i,\gamma}c^*_{\lambda_i}c_{\lambda'_i}\left[A^j_{\lambda_i,\gamma}A^{j'}_{\gamma,\lambda'_i} + A^{j'}_{\lambda_i,\gamma}A^j_{\gamma,\lambda'_i}\right] \\ &- \frac{e^2}{h}\left(\sum_{\lambda_i,\lambda'_i}c^*_{\lambda_i}c_{\lambda'_i}A^j_{\lambda_i,\lambda'_i}\right)\left(\sum_{\lambda_i,\lambda'_i}c^*_{\lambda_i}c_{\lambda'_i}A^{j'}_{\lambda_i,\lambda'_i}\right), \quad \text{(A15)} \end{aligned}$$

with indices λ_i,λ'_i bound to lead i.

Within the Born approximation we obtain for the cross-correlators, with implicit summation over all indices (summation within each bracket in both second lines),

$$S_{\text{sp,1}}^{34} = \frac{e^2}{h} \text{Re}\big\{ c_{1,\tau_1,\nu}^* c_{1,\tau_1',\nu} \big[T_{3,\tau_1,\nu} r_{(4,\tau_4,\nu_4),(1,\tau_1,\nu)}^* r(4,\tau_4,\nu_4),(1,\tau_1',\nu) + t_{(3,\tau_1,\nu)}^* t_{(4,\tau_2,\nu_2)}^* r(3,\tau_1,\nu),(2,\tau_2,\nu_2) r(4,\tau_2,\nu_2),(1,\tau_1',\nu) \big] \big\}$$

$$- \frac{e^2}{h} \big[|c_{1,\tau_1,\nu}|^2 T_{3,\tau_1,\nu} \big] \big[c_{1,\tau_1,\nu}^* c_{1,\tau_1',\nu} r_{(4,\tau_4,\nu_4),(1,\tau_1,\nu)}^* r(4,\tau_4,\nu_4),(1,\tau_1'\nu) \big], \tag{A16}$$

$$S_{\text{sp,2}}^{34} = \frac{e^2}{h} \text{Re}\big\{ c_{2,\tau_2,\nu}^* c_{2,\tau_2',\nu} \big[T_{4,\tau_2',\nu} r_{(3,\tau_3,\nu_3),(2,\tau_2,\nu)}^* r(3,\tau_3,\nu_3),(2,\tau_2',\nu) + t_{(3,\tau_3,\nu_3)}^* t_{(4,\tau_1,\nu)}^* r(3,\tau_3,\nu_3),(2,\tau_2',\nu) r(4,\tau_2,\nu),(1,\tau_3,\nu_3) \big] \big\}$$

$$- \frac{e^2}{h} \big[|c_{2,\tau_2,\nu}|^2 T_{4,\tau_2,\nu} \big] \big[c_{2,\tau_2,\nu}^* c_{2,\tau_2',\nu} r_{(3,\tau_3,\nu_3),(2,\tau_2,\nu)}^* r(3,\tau_3,\nu_3),(2,\tau_2',\nu) \big], \tag{A17}$$

$t_{3,\tau,\nu} = t_{(3,\tau,\nu),(1,\tau,\nu)}, t_{4,\tau,\nu} = t_{(4,\tau,\nu),(2,\tau,\nu)}, T_{3,\tau,\nu} = |t_{3,\tau,\nu}|^2$, and $T_{4,\tau,\nu} = |t_{4,\tau,\nu}|^2$.

Specializing, for instance, to the wave functions $|\Psi_{i,\nu_0}\rangle$ defined by the amplitudes $c_{i,\tau,\nu} = \delta_{\nu,\nu_0}/\sqrt{2}$ allows us to capture the injection of a spin ν_0 into lead i with equal weights in both valleys.

APPENDIX B: DEMONSTRATION THAT $S^{33} = -S^{34}$ IN THE ABSENCE OF BACKSCATTERING

In the absence of backscattering into the incoming leads $i = 1,2$, described by a scattering matrix as in Eq. (5), any injected particles are fully transmitted into the outgoing leads $i = 3,4$. Hence, by particle conservation (the unitarity of the scattering matrix), $I^3 + I^4 = -\hat{N}_{\text{in}}$, where $\hat{N}_{\text{in}} = \sum_{i=1,2,\tau,\nu,\epsilon} a_{i,\tau,\nu,\epsilon}^\dagger a_{i,\tau,\nu,\epsilon}$ counts the number of incoming particles. Therefore, for any state $|\Psi\rangle$ with a number N of incoming particles, $\hat{N}_{\text{in}}|\Psi\rangle = N|\Psi\rangle$ and $\langle\Psi|\{I^3,(I^3 + I^4)\}|\Psi\rangle = -2N\langle\Psi|I^3|\Psi\rangle = 2\langle\Psi|I^3|\Psi\rangle\langle\Psi|(I^3 + I^4)|\Psi\rangle$. Consequently $S^{33} + S^{34} = \frac{1}{2}\langle\Psi|\{I^3,(I^3 + I^4)\}|\Psi\rangle - \langle\Psi|I^3|\Psi\rangle\langle\Psi|(I^3 + I^4)|\Psi\rangle = 0$. By precisely the same argument $S^{44} + S^{34} = 0$, and therefore $S^{33} = S^{44}$.

These identities are independent of whether $|\Psi\rangle$ is entangled or not, but the provided proof depends on the absence of backscattering in the scattering matrix, Eq. (5).

[1] S. J. Tans, M. H. Devoret, H. Dai, A. Thess, R. E. Smalley, L. J. Geerligs, and C. Dekker, Nature (London) **386**, 474 (1997).

[2] D. H. Cobden and J. Nygård, Phys. Rev. Lett. **89**, 046803 (2002).

[3] W. Liang, M. Bockrath, and H. Park, Phys. Rev. Lett. **88**, 126801 (2002).

[4] E. Minot, Y. Yaish, V. Sazonova, and P. McEuen, Nature (London) **428**, 536 (2004).

[5] P. Jarillo-Herrero, S. Sapmaz, C. Dekker, L. P. Kouwenhoven, and H. S. J. van der Zant, Nature (London) **429**, 389 (2004).

[6] P. Jarillo-Herrero, J. Kong, H. S. J. van der Zant, C. Dekker, L. P. Kouwenhoven, and S. De Franceschi, Phys. Rev. Lett. **94**, 156802 (2005).

[7] M. R. Gräber, W. A. Coish, C. Hoffmann, M. Weiss, J. Furer, S. Oberholzer, D. Loss, and C. Schönenberger, Phys. Rev. B **74**, 075427 (2006).

[8] A. Vijayaraghavan, J. Mater. Chem. **22**, 7083 (2012).

[9] H. Park, A. Afzali, S.-J. Han, G. S. Tulevski, A. D. Franklin, J. Tersoff, J. B. Hannon, and W. Haensch, Nature Nanotechnol. **7**, 787 (2012).

[10] L. G. Hermann, F. Portier, P. Roche, A. Levy Yeyati, T. Kontos, and C. Strunk, Phys. Rev. Lett. **104**, 026801 (2010).

[11] J. Schindele, A. Baumgartner, and C. Schönenberger, Phys. Rev. Lett. **109**, 157002 (2012).

[12] P. Recher, E. V. Sukhorukov, and D. Loss, Phys. Rev. B **63**, 165314 (2001).

[13] L. Hofstetter, S. Csonka, J. Nygård, and C. Schönenberger, Nature (London) **461**, 960 (2009).

[14] L. Hofstetter, S. Csonka, A. Baumgartner, G. Fülöp, S. d'Hollosy, J. Nygård, and C. Schönenberger, Phys. Rev. Lett. **107**, 136801 (2011).

[15] A. Das, Y. Ronen, M. Heiblum, D. Mahalu, A. V. Kretinin, and H. Shtrikman, Nature Commun. **3**, 1165 (2012).

[16] J. Torrès and T. Martin, Eur. Phys. J. B **12**, 319 (1999).

[17] G. Deutscher and D. Feinberg, Appl. Phys. Lett. **76**, 487 (2000).

[18] G. Lesovik, T. Martin, and G. Blatter, Eur. Phys. J. B **24**, 287 (2001).

[19] P. Recher and D. Loss, Phys. Rev. B **65**, 165327 (2002).

[20] C. Bena, S. Vishveshwara, L. Balents, and M. P. A. Fisher, Phys. Rev. Lett. **89**, 037901 (2002).

[21] P. Recher and D. Loss, Phys. Rev. Lett. **91**, 267003 (2003).

[22] X. Hu and S. Das Sarma, Phys. Rev. B **69**, 115312 (2004).

[23] P. Samuelsson, E. V. Sukhorukov, and M. Büttiker, Phys. Rev. B **70**, 115330 (2004).

[24] O. Sauret, T. Martin, and D. Feinberg, Phys. Rev. B **72**, 024544 (2005).

[25] K. V. Bayandin, G. B. Lesovik, and T. Martin, Phys. Rev. B **74**, 085326 (2006).

[26] T. Ando, J. Phys. Soc. Jpn. **69**, 1757 (2000).

[27] L. Chico, M. P. López-Sancho, and M. C. Muñoz, Phys. Rev. Lett. **93**, 176402 (2004).

[28] D. Huertas-Hernando, F. Guinea, and A. Brataas, Phys. Rev. B **74**, 155426 (2006).

[29] W. Izumida, K. Sato, and R. Saito, J. Phys. Soc. Jpn. **78**, 074707 (2009).

[30] J.-S. Jeong and H.-W. Lee, Phys. Rev. B **80**, 075409 (2009).

[31]L. Chico, M. P. López-Sancho, and M. C. Muñoz, Phys. Rev. B **79**, 235423 (2009).

[32]J. Klinovaja, M. J. Schmidt, B. Braunecker, and D. Loss, Phys. Rev. Lett. **106**, 156809 (2011).

[33]J. Klinovaja, M. J. Schmidt, B. Braunecker, and D. Loss, Phys. Rev. B **84**, 085452 (2011).

[34]M. del Valle, M. Margańska, and M. Grifoni, Phys. Rev. B **84**, 165427 (2011).

[35]L. Chico, H. Santos, M. C. Muñoz, and M. P. López-Sancho, Solid State Commun. **152**, 1477 (2012).

[36]D. V. Bulaev, B. Trauzettel, and D. Loss, Phys. Rev. B **77**, 235301 (2008).

[37]S. Weiss, E. I. Rashba, F. Kuemmeth, H. O. H. Churchill, and K. Flensberg, Phys. Rev. B **82**, 165427 (2010).

[38]P. Burset, W. Herrera, and A. Levy Yeyati, Phys. Rev. B **84**, 115448 (2011).

[39]A. Cottet, T. Kontos, and A. Levy Yeyati, Phys. Rev. Lett. **108**, 166803 (2012).

[40]A. Cottet, Phys. Rev. B **86**, 075107 (2012).

[41]B. Braunecker, P. Burset and A. Levy Yeyati, Phys. Rev. Lett. **111**, 136806 (2013).

[42]F. Kuemmeth, S. Ilani, D. C. Ralph, and P. L. McEuen, Nature (London) **452**, 448 (2008).

[43]T. S. Jespersen, K. Grove-Rasmussen, K. Flensberg, J. Paaske, K. Muraki, T. Fujisawa, and J. Nygård, Phys. Rev. Lett. **107**, 186802 (2011).

[44]G. A. Steele, F. Pei, E. A. Laird, J. M. Jol, H. B. Meerwaldt, and L. P. Kouwenhoven, Nature Commun. **4**, 1573 (2013).

[45]H. W. Ch. Postma, M. de Jonge, Z. Yao, and C. Dekker, Phys. Rev. B **62**, R10653 (2000).

[46]M. S. Fuhrer, J. Nygård, L. Shih, M. Forero, Y. G. Yoon, M. S. C. Mazzoni, H. J. Choi, J. Ihm, S. G. Louie, A. Zettl, and P. L. McEuen, Science **288**, 494 (2000).

[47]J. Kim, K. Kang, J.-O. Lee, K.-H. Yoo, J.-R. Kim, J. W. Park, H. M. So, and J.-J. Kim, J. Phys. Soc. Jpn. **70**, 1464 (2001).

[48]J. W. Janssen, S. G. Lemay, L. P. Kouwenhoven, and C. Dekker, Phys. Rev. B **65**, 115423 (2002).

[49]N. Yoneya, K. Tsukagoshi, and Y. Aoyagi, Appl. Phys. Lett. **81**, 2250 (2002).

[50]J. W. Park, J. Kim, and K.-H. Yoo, J. Appl. Phys. **93**, 4191 (2003).

[51]B. Gao, A. Komnik, R. Egger, D. C. Glattli, and A. Bachtold, Phys. Rev. Lett. **92**, 216804 (2004).

[52]Y.-G. Yoon, M. S. C. Mazzoni, H. J. Choi, J. Ihm, and S. G. Louie, Phys. Rev. Lett. **86**, 688 (2001).

[53]T. Nakanishi and T. Ando, J. Phys. Soc. Jpn. **70**, 1647 (2001).

[54]A. Komnik and R. Egger, Eur. Phys. J. B **19**, 271 (2001).

[55]S. Dag, R. T. Senger, and S. Ciraci, Phys. Rev. B **70**, 205407 (2004).

[56]V. Margulis and M. Pyataev, Phys. Rev. B **76**, 085411 (2007).

[57]P. Havu, M. J. Hashemi, M. Kaukonen, E. T. Seppälä, and R. M. Nieminen, J. Phys.: Condens. Matter **23**, 112203 (2011).

[58]G. Burkard, D. Loss, and E. V. Sukhorukov, Phys. Rev. B **61**, R16303 (2000).

[59]J. C. Egues, G. Burkard, and D. Loss, Phys. Rev. Lett. **89**, 176401 (2002).

[60]J. C. Egues, G. Burkard, D. S. Saraga, J. Schliemann, and D. Loss, Phys. Rev. B **72**, 235326 (2005).

[61]P. San-Jose and E. Prada, Phys. Rev. B **74**, 045305 (2006).

[62]S. Kawabata, J. Phys. Soc. Jpn. **70**, 1210 (2001).

[63]N. M. Chtchelkatchev, G. Blatter, G. B. Lesovik, and T. Martin, Phys. Rev. B **66**, 161320(R) (2002).

[64]P. Samuelsson, E. V. Sukhorukov, and M. Büttiker, Phys. Rev. Lett. **91**, 157002 (2003).

[65]L. Faoro and F. Taddei, Phys. Rev. B **75**, 165327 (2007).

[66]P. Samuelsson and M. Büttiker, Phys. Rev. B **73**, 041305 (2006).

[67]R. Saito, G. Dresselhaus, and M. S. Dresselhaus, *Physical Properties of Carbon Nanotubes* (Imperial College Press, London, 1998).

[68]J. Serrano, M. Cardona, and J. Ruf, Solid State Commun. **113**, 411 (2000).

[69]H. Min, J. E. Hill, N. A. Sinitsyn, B. R. Sahu, L. Kleinman, and A. H. MacDonald, Phys. Rev. B **74**, 165310 (2006).

[70]F. Guinea, New J. Phys. **12**, 083063 (2010).

[71]M. Büttiker, Phys. Rev. B **46**, 12485 (1992).

[72]S.-H. Jhang, M. Margańska, M. del Valle, Y. Skourski, M. Grifoni, J. Wosnitza, and C. Strunk, Phys. Status Solidi B **248**, 2672 (2011).

[73]K. Flensberg and C. M. Marcus, Phys. Rev. B **81**, 195418 (2010).

[74]F. Pei, E. A. Laird, G. A. Steele, and L. P. Kouwenhoven, Nature Nanot. **7**, 630 (2012).

[75]E. A. Laird, F. Pei, and L. P. Kouwenhoven, Nature Nanotechnol. **8**, 565 (2013).

[76]R. A. Lai, H. O. H. Churchill, and C. M. Marcus, arXiv:1210.6402.

[77]For the proposal of Ref. 12, ϵ_0 is determined by the quantum dot resonances. To avoid interaction with the underlying Fermi sea of the normal leads, which potentially could destroy the entanglement of the injected pair, we should still have $\epsilon_0 - \epsilon_F > k_B T, \Gamma_{\text{inj}}$, with Γ_{inj} the tunneling rates from the quantum dots to the normal leads (Ref. 12).